Journal of Sound and Vibration (2002) **250**(3), 541–565
doi:10.1006/jsvi.2001.3950, available online at http://www.idealibrary.com on IDEAL®

COINCIDENCE OF THERMOELASTIC AND THERMOVISCOUS ACOUSTIC WAVES IN FLUID-FILLED ELASTIC TUBES

P. N. Liang

Harley-Davidson Motor Co., 11800 W. Capitol Dr., Wauwatosa, WI 53222, U.S.A.
E-mail: paul_liang@harley-davidson.com

AND

H. A. Scarton

Laboratory for Noise and Vibration Control Research, Department of Mechanical, Aerospace, and Nuclear Engineering, Rensselaer Polytechnic Institute, Troy, NY 12180-3590, U.S.A.
E-mail: scarton@rpi.edu

(*Received* 7 *May* 2001, *and in final form* 17 *August* 2001)

Thermoelastic and thermoviscous acoustic wave propagation in fluid-filled steel tubes is studied using the exact three-dimensional (3-D) fluid-elastic coupled system equations for the vibration in the $n = 0$ and 1 circumferential modes. Water- and air-filled tubes are examined. The water-filled steel tube shows a strong fluid–elastic coupling effect in the lower frequency range and the air-filled tube shows a strong thermal effect for all frequencies. An 88·9 mm outer diameter tube with 3·05 mm wall thickness is used for the study. Due to the fluid–elastic coupling introduced for air having a specific heat ratio of 1·4 (the solution uncouples when the ratio is 1·0), thermal effects are seen to be very important with the modal attenuation rate being at least 32% underestimated if the thermal effect is not included in the air–steel system. A coincidence phenomenon is accurately found directly from the coupled modes in the fluid–elastic coupled system. When coincidence occurs, the axial modal attenuation rate drops sharply, allowing the exact determination of the coincidence frequency by locating the local minimum of the modal spatial attenuation rate with increasing frequency. In the water–steel system, the coincidence frequency is seen to be 8% in error if methods are employed using the uncoupled theory for the separate fluid and elastic wall.

1. INTRODUCTION

For waves propagating in a fluid-filled tube, a resonance is possible if the axial wave speeds in the fluid column and the elastic tube are the same. This strong interaction between the fluid column and its elastic tube containment vessel is called *coincidence*. An approximate coincidence frequency can be estimated by using the uncoupled method, that is, finding the same wave speeds in an elastic system and a fluid system [1, 2]. This method may be more appropriate for a nearly uncoupled system such as an air-filled tube; although the thermal effect will be seen to be very prominent in the modal attenuation rate of the air–steel coupled system. For a water-filled tube, the fluid and the elastic systems have strongly interacted and must be treated as a coupled system.

The fluid–elastic coupled system has been studied by several authors. Lamb [3] was probably the first one to investigate the propagation of sound waves in tubes as affected by

0022-460X/02/080541 + 25 $35.00/0

the elasticity of the walls. Thomson [4] examined the axially symmetric wave propagation ($n = 0$) in a water-filled brass thin tube, including the effects of inertia, stiffness, and the Poisson ratio. The effect of viscosity on propagation was calculated by assuming the viscosity to be small and utilizing the velocity distribution of the inviscid solution. Thomson only found one mode near zero frequency. Thomson erroneously concluded that the mode starting at the first cut-off frequency has the least energy dissipation (i.e., the least-attenuated mode and is called P30C mode in this paper); thus this mode will predominate the frequencies higher than the first cut-off frequency. Unfortunately, Thomson missed the other important coupled mode near the zero frequency (as mentioned by Lin and Morgan [5]; it is called the P20C mode in this paper), which is the least-attenuated mode with increasing frequency until the fourth coupled mode emerges (the P40C mode defined in this paper).

Lin and Morgan [5] investigated the propagation of axially symmetric waves ($n = 0$) in compressible inviscid fluid ($v_0 = 0$) contained in a cylindrical, elastic shell. They tried to improve the results in higher frequencies by adding the transverse shear and the rotational inertia of the tube. They concluded that the influence of rotatory inertia is unimportant even at high frequencies; the transverse shear is of importance only for the lowest mode where it tends to reduce the phase velocity.

Kumar [6] studied the dispersion of axially symmetric waves in empty and fluid-filled circular cylindrical tubes for various thicknesses. Instead of using shell theory for the elastic tube, Kumar's dispersion relation is based upon exact 3-D elasticity. Kumar was also the first to construct imaginary and complex modes of the dispersion curves corresponding to axially symmetric waves in an inviscid fluid-filled elastic tube. Fuller and Fahy [7] investigated the dispersion of axially symmetric waves ($n = 0$) and higher order circumferential non-axially symmetric waves ($n = 1$) in an inviscid fluid-filled elastic thin shell. Fahy [2] suggested estimating the coincidence frequency by determining that frequency wherein the axial phase speeds of each pure fluid mode in the uncoupled state equal each corresponding phase velocity of the purely elastic wall uncoupled modes. In this paper, the coincidence frequency is determined directly from the fluid–elastic coupled system by first finding the frequency corresponding to the local minimum of the modal spatial attenuation rate. Note that not all the local minimum attenuation rates are caused by the coincidence phenomenon. The fluid modes at the cut-off frequencies also have the local minimum of the attenuation rates even in a fluid-alone system as discussed in section 5.1.

Chang *et al.* [8] have removed the thin shell assumption and used the exact 3-D dispersion equations of axially symmetric ($n = 0$) and non-axially symmetric ($n = 1$) waves in a viscous liquid-filled elastic tube. None of these authors considered the thermal effect. One of the objectives of this study is to expand the Chang *et al.* work to include the thermal effect in the fluid–elastic coupled system equations and to more fully expand the exact understanding of modal coincidence.

2. SYSTEM EQUATIONS

The system equations for the elastic system and the fluid system were fully derived and presented in our previous work [9, 10] and are summarized below. In the thermoelastic tube, the "corrected" heat conduction equation and the Navier–Cauchy momentum equation are, respectively [9],

$$k_s \nabla^2 T = \rho_s c_v \partial_t T + \beta_s T_0 \partial_t \varepsilon_{\alpha\alpha}, \quad \varepsilon_{\alpha\alpha} = \varepsilon_{rr} + \varepsilon_{\theta\theta} + \varepsilon_{zz} = \nabla \cdot \mathbf{u}, \tag{1a, b}$$

$$\rho_s \partial_t^2 \mathbf{u} = \mu \nabla^2 \mathbf{u} + (\lambda + \mu) \nabla(\nabla \cdot \mathbf{u}) - \beta_s \nabla T. \tag{2}$$

In the thermoviscous fluid column without net flow, the continuity equation, Navier–Stokes momentum equation, thermodynamic energy equation, two modified state equations are, respectively [10],

$$\textit{Continuity equation}: \partial_t \rho + \rho_0 \nabla \cdot \mathbf{v} = 0, \tag{3}$$

$$\textit{Navier–Stokes equation}: \partial_t \mathbf{v} = -\frac{1}{\rho_0}\nabla P - \nu_0 \nabla \times \nabla \times \mathbf{v} + (\nu_0' + \tfrac{4}{3}\nu_0)\nabla(\nabla \cdot \mathbf{v}), \tag{4}$$

$$\textit{Thermodynamic energy equation}: \rho_0 T_0 \partial_t s = k_f \nabla^2 T \tag{5}$$

and the two modified state equations are

$$\rho = \frac{1}{C_0^2}\left\{P - \rho_0 C_0 \left[\frac{(\gamma_0 - 1)T_0}{c_p}\right]^{1/2} s\right\}, \tag{6}$$

$$T = \frac{C_0}{\rho_0}\left[\frac{(\gamma_0 - 1)T_0}{c_p}\right]^{1/2} \rho + \frac{\gamma_0 T_0}{c_p} s. \tag{7}$$

The coupled system closed-form solutions for the displacements $\mathbf{u}$, velocities $\mathbf{v}$ and temperature T are identical to the elastic-alone, and the fluid-alone, systems detailed in our previous work [9, 10]. At a given frequency, the eigenvalues (modal wave numbers) and the corresponding eigenvectors (mode shapes) are found from the coupled system equations by equating the boundary conditions between the fluid column and the elastic tube.

All the above notations were used in our previous work in the elastic-alone tube [9] and the fluid-alone column [10] except the reference radius and the reference modal phase speed when deriving the dimensionless variables. In this fluid–elastic coupled system, the reference radius is the *outer* radius of the tube, while the inner tube radius was the reference radius for the fluid-alone system [10] since the tube does not exist in the fluid-alone system. The reference-phase speed here is the intrinsic plane wave speed C_0 of the *unbounded fluid medium*, while the transverse wave speed of the elastic tube is the reference-phase speed for the elastic-alone system in reference [9] as well as in the fluid–elastic coupled system presented in the Ph.D. Thesis of Liang [11].

3. BOUNDARY CONDITIONS OF THE FLUID–ELASTIC SYSTEM

Twelve radial boundary conditions form 12 homogeneous linear equations in those 12 unknown amplitude coefficients. These 12 equations construct a 12×12 determinant and lead to a characteristic equation. Four of these boundary conditions come from satisfying the conditions at the outer tube wall a in Figure 1, and eight from the inner tube wall b. On the outer tube wall, these are, respectively, three free stresses and one natural convection from the tube to the ambient air with its associated thermal conductivity of the elastic tube (also known as Newton's cooling law):

$$\tau_{rr} = \tau_{rz} = \tau_{r\theta} = 0, \quad k_s \partial_r T + h_f T = 0 \quad (\text{at } r = a), \tag{8a–d}$$

In the tube inside the surface interfacing directly with the fluid, there are, respectively, three continuous components of stress, three continuous components of displacement,

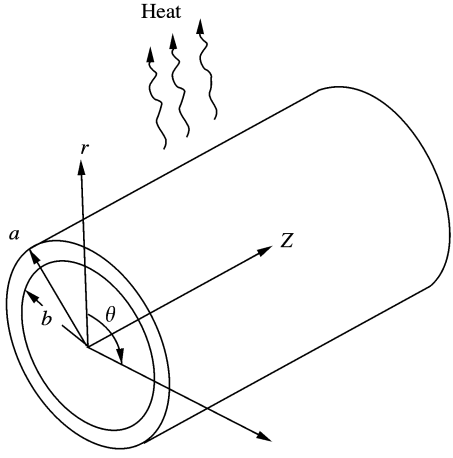

Figure 1. Geometry and co-ordinate system of a fluid-filled tube with free air convection on the outer tube. The outer and inner radii are 0·04445 and 0·04140 m respectively. The radius ratio ($\mathbb{R} = b/a$) is 0·93138.

continuity of temperature and continuity of heat flux:

$$(\tau_{rr})_s = (\tau_{rr})_f, \quad (\tau_{rz})_s = (\tau_{rz})_f, \quad (\tau_{r\theta})_s = (\tau_{r\theta})_f \ (\text{at } r = b), \tag{9a–c}$$

$$u_r = v_r/\mathrm{i}\omega, \quad u_z = v_z/\mathrm{i}\omega, \quad u_\theta = v_\theta/\mathrm{i}\omega \ (\text{at } r = b), \tag{10a–c}$$

$$(T)_s = (T)_f \quad \text{and} \quad k_s\, \partial_r(T)_s = k_f\, \partial_r(T)_f \ (\text{at } r = b). \tag{11a,b}$$

The subscripts $(\ )_s$ and $(\ )_f$ in equations (9) and (11) stand for the thermoelastic solid and the thermoviscous fluid systems respectively. Imposing these 12 radial boundary conditions results in the matrix form

$$\mathbf{D} \cdot \mathbf{L} = \mathbf{0}, \tag{12}$$

where the eigenvector $\mathbf{L}^{\mathrm{T}}$ contains the modal amplitudes $\mathbf{L}^{\mathrm{T}} = [A_1, B_1, A_2, B_2, E, F, G, H, C_1, C_2, Q, S]$ and $\mathbf{D}$ is a 12×12 coefficient matrix for the fluid–elastic coupled system. A non-trivial solution of $\mathbf{L}$ requires the determinant of coefficient matrix $\mathbf{D}$ to equal zero, which leads to the characteristic equation

$$\det [D_{jk}] = 0, \quad j \ (\text{and } k) = 1, 2, \ \ldots\ , 12. \tag{13}$$

The 12×12 matrix of $\mathbf{D}$ is shown in Table 1 and the detailed expression of each element in Table 1 is listed in Appendix A in dimensionless form.

The full matrix shown in Table 1 corresponds to the fluid–elastic coupled system including both non-axially symmetric waves and the thermal effect. If the thermal effect is neglected (by setting the ratio of specific heats γ_0 to 1), then the 12×12 matrix reduces to a 9×9 matrix [8]. The system is reduced in size further by imposing an axial symmetry giving a 6×6 matrix. Similarly, the thermoelastic waves in an empty tube reduce to an 8×8, and the thermoviscous acoustic waves in fluid lines to a 4×4 matrix [9, 10]. Finally, for an axially symmetric viscous compressible fluid in a rigid, impermeable tube, the system reduces to a 2×2 matrix [12]. Table 2 summarizes these reduced systems.

TABLE 1

A 12×12 *matrix for the complete coupled system with thermal effect*

B.C.	Elastic tube								Fluid line			
Stress	*On the outer surface,* $r = a$											
$(\tau_{rr})_s = 0$	$D_{1,1}$	$D_{1,2}$	$D_{1,3}$	$D_{1,4}$	$D_{1,5}$	$D_{1,6}$	$D_{1,7}$	$D_{1,8}$	0	0	0	0
$(\tau_{rz})_s = 0$	$D_{2,1}$	$D_{2,2}$	$D_{2,3}$	$D_{2,4}$	$D_{2,5}$	$D_{2,6}$	$D_{2,7}$	$D_{2,8}$	0	0	0	0
$(\tau_{r\theta})_s = 0$	$D_{3,1}$	$D_{3,2}$	$D_{3,3}$	$D_{3,4}$	$D_{3,5}$	$D_{3,6}$	$D_{3,7}$	$D_{3,8}$	0	0	0	0
Temperature												
$k_s\partial_r T + h_f T = 0$	$D_{4,1}$	$D_{4,2}$	$D_{4,3}$	$D_{4,4}$	0	0	0	0	0	0	0	0
Stress	*At the fluid–solid interface,* $r = b$											
$(\tau_{rr})_s = (\tau_{rr})_f$	$D_{5,1}$	$D_{5,2}$	$D_{5,3}$	$D_{5,4}$	$D_{5,5}$	$D_{5,6}$	$D_{5,7}$	$D_{5,8}$	$D_{5,9}$	$D_{5,10}$	$D_{5,11}$	$D_{5,12}$
$(\tau_{rz})_s = (\tau_{rz})_f$	$D_{6,1}$	$D_{6,2}$	$D_{6,3}$	$D_{6,4}$	$D_{6,5}$	$D_{6,6}$	$D_{6,7}$	$D_{6,8}$	$D_{6,9}$	$D_{6,10}$	$D_{6,11}$	$D_{6,12}$
$(\tau_{r\theta})_s = (\tau_{r\theta})_f$	$D_{7,1}$	$D_{7,2}$	$D_{7,3}$	$D_{7,4}$	$D_{7,5}$	$D_{7,6}$	$D_{7,7}$	$D_{7,8}$	$D_{7,9}$	$D_{7,10}$	$D_{7,11}$	$D_{7,12}$
Displacement												
$u_r = v_r/\mathrm{i}\omega$	$D_{8,1}$	$D_{8,2}$	$D_{8,3}$	$D_{8,4}$	$D_{8,5}$	$D_{8,6}$	$D_{8,7}$	$D_{8,8}$	$D_{8,9}$	$D_{8,10}$	$D_{8,11}$	$D_{8,12}$
$u_z = v_z/\mathrm{i}\omega$	$D_{9,1}$	$D_{9,2}$	$D_{9,3}$	$D_{9,4}$	$D_{9,5}$	0	$D_{9,7}$	0	$D_{9,9}$	$D_{9,10}$	$D_{9,11}$	0
$u_\theta = v_\theta/\mathrm{i}\omega$	$D_{10,1}$	$D_{10,2}$	$D_{10,3}$	$D_{10,4}$	$D_{10,5}$	$D_{10,6}$	$D_{10,7}$	$D_{10,8}$	$D_{10,9}$	$D_{10,10}$	$D_{10,11}$	$D_{10,12}$
Temperature												
$(T)_s = (T)_f$	$D_{11,1}$	$D_{11,2}$	$D_{11,3}$	$D_{11,4}$	0	0	0	0	$D_{11,9}$	$D_{11,10}$	0	0
$k_s\partial_r(T)_s = k_f\partial_r(T)_f$	$D_{12,1}$	$D_{12,2}$	$D_{12,3}$	$D_{12,4}$	0	0	0	0	$D_{12,9}$	$D_{12,10}$	0	0

TABLE 2

Reduced matrices for different wave propagation cases

Case	System	Dimensions	Circum., n	Thermal	$D_{j,k}$
1	Coupled	12×12	$n = 1$	Yes	$j = 1$–12; $k = 1$–12
2	Coupled	9×9	$n = 0$	Yes	$j = 1, 2, 4, 5, 6, 8, 9, 11, 12$; $k = 1, 2, 3, 4, 5, 7, 9, 10, 11$
3	Coupled	9×9	$n = 1$	No	$j = 1$–3, 5–10; $k = 1, 2, 5$–9, 11, 12
4	Coupled	6×6	$n = 0$	No	$j = 1, 2, 5, 6, 8, 9$; $k = 1, 2, 5, 7, 9, 11$
5	Elastic	8×8	$n = 1$	Yes	$j = 1$–7, 12; $k = 1$–8
6	Elastic	6×6	$n = 0$	Yes	$j = 1, 2, 4, 5, 6, 12$; $k = 1$–5, 7
7	Elastic	6×6	$n = 1$	No	$j = 1$–3, 5–7; $k = 1, 2, 5$–8
8	Elastic	4×4	$n = 0$	No	$j = 1, 2, 5, 6$; $k = 1, 2, 5, 7$
9	Fluid	4×4	$n = 1$	Yes	$j = 8, 9, 10, 12$; $k = 9$–12
10	Fluid	3×3	$n = 0$	Yes	$j = 8, 9, 12$; $k = 9$–11
11	Fluid	3×3	$n = 1$	No	$j = 8, 9, 10$; $k = 9, 11, 12$
12	Fluid	2×2	$n = 0$	No	$j = 8, 9$; $k = 9, 11$

4. WATER- AND AIR-FILLED STEEL TUBES

In motorcycle muffler acoustic designs, the study of an air-filled pipe system is more useful than a water-filled tube. However, since water has a higher density and a wave speed similar in magnitude to the steel wall wave speeds than air, its fluid–elastic coupling effect will be stronger than air. Therefore, the water-filled tube will be studied first for both axially symmetric and non-axially symmetric modes; the air-filled tube, whose principal importance lies in the stronger thermal effect will be examined in lesser detail by examining only its axially symmetric mode to show the importance of the thermal effect.

Water at room temperature (20°C or 293 K) has the following properties: $\rho_0 = 998\ \text{kg/m}^3$, shear viscosity $\mu_0 = 0{\cdot}001\ \text{kg/(m s)}$, ratio of specific heat $\gamma_0 = 1{\cdot}004$, specific heat at constant pressure $c_p = 4181\ \text{J/(kg K)}$, and thermal conductivity of fluid $k_f = 0{\cdot}556\ \text{W/(m K)}$. The intrinsic longitudinal plane-wave phase speed of water at room temperature, C_0, is 1481 m/s.

The air at room temperature has the following properties: $\rho_0 = 1{\cdot}21\ \text{kg/m}^3$, shear viscosity $\mu_0 = 1{\cdot}81 \times 10^{-5}\ \text{kg/(m s)}$, ratio of specific heat $\gamma_0 = 1{\cdot}402$, specific heat at constant pressure $c_p = 1005.6\ \text{J/(kg K)}$, and thermal conductivity of fluid $k_f = 0{\cdot}02568\ \text{W/(m K)}$. The intrinsic plane-wave phase speed of air at room temperature, C_0, is 343 m/s.

The tube used for the calculations is made of steel. The respective outer and inner radii of the tube are $a = 44{\cdot}45$ mm and $b = 41{\cdot}40$ mm, as shown in Figure 1. The radius ratio ($\mathbb{R} = b/a$) is 0·93138. The tube is assumed to be infinitely long, oriented horizontally in an equilibrium condition. The water flow is zero and the equilibrium temperature $T_0 = 293$ K (20°C). It should be noted that the previous work [9] used an aluminium tube with 20 and 10 mm outer and inner radii.

The steel tube used in this paper at room temperature has the following material properties: the Poisson ratio $\nu = 0{\cdot}28$, Young's modulus $E = 195$ GPa, mass density $\rho_s = 7700\ \text{kg/m}^3$; coefficient of linear thermal expansion $\alpha_s = 1{\cdot}1 \times 10^{-5}\ \text{m/(m K)}$, thermal conductivity of solid $k_s = 54\ \text{W/(m K)}$, specific heat at constant volume $c_v = 465\ \text{J/(kg K)}$, convection heat transfer coefficient of free-convection of air over a horizontal pipe $h_f = 6{\cdot}5\ \text{W/(m}^2\,\text{K)}$ [11]. The pure longitudinal-wave (i.e., one-dimensional wave propagation in an infinite solid medium; dilatation without lateral strain [2]), transverse-wave and torsional-wave phase speeds are calculated as $C_d = 5690$ m/s and $C_t = 3145$ m/s, $C_q = 3145$ m/s respectively. When the tube geometry is circular, the torsional-wave phase speed is the same as the shear-wave phase speed [13]. The corresponding dimensionless phase speeds (i.e., $C_D = C_d/C_o$, $C_T = C_t/C_o$, and $C_Q = C_q/C_o$) in the water–steel system are 3·84, 2·12 and 2·12 respectively. The corresponding dimensionless phase speeds in the air–steel system are 16·6, 9·17 and 9·17.

The dimensionless frequency of interest $\Omega (= \omega a/C_o$, where $a = 0{\cdot}04445$ m) is studied in the range $0{\cdot}01 \leqslant \Omega \leqslant 12$, which corresponds to 53–63 633 Hz in the water system and 12–14 733 Hz in the air system. Three-dimensional mode shapes in terms of displacement of the wave propagation along the z direction can be plotted according to the formula:

$$\mathbf{u}(R, \theta, Z; \tau) = \text{Re}\,[\mathbf{U}(R)\mathrm{e}^{\mathrm{i}n\theta + \zeta Z}\mathrm{e}^{\mathrm{i}\Omega\tau}], \tag{14}$$

where $\mathbf{U}(R) = U_r(R)\mathbf{e}_r + U_\theta(R)\mathbf{e}_\theta + U_z(R)\mathbf{e}_z$, n is the circumferential mode number; $\zeta (= ka)$ is a dimensionless complex wave number in the axial direction, $\zeta = \zeta_r + \mathrm{i}\zeta_i$; $R = r/a$ and $Z = z/\lambda$ are the dimensionless radial and axial co-ordinates; and Ω and τ, the dimensionless frequency and time respectively. Due to the similarity of the real and imaginary parts of the spatial mode shapes (those not associated with the temporal part of the solution $\mathrm{e}^{\mathrm{i}\Omega\tau}$), only the real part of the spatial mode shapes will be plotted and discussed.

The real part ζ_r is the dimensionless axial modal attenuation rate or attenuation constant, and the imaginary part ζ_i, is the dimensionless axial modal propagation constant. The dimensionless axial modal phase velocity can be calculated through the propagation constant as $C^* = C/C_0 = \Omega/\zeta_i$. The attenuation rates of the propagating modes are nearly zero ($\zeta_r < 0{\cdot}001$). The complex modes having higher axial attenuation rates ($\zeta_r > 0{\cdot}1$) are often referred to as the evanescent waves. Evanescent waves are only important for the nearfield measurement, such as a microphone sensing the signal near the piston actuator for the active noise control in a tube waveguide [14]. In this paper, we are mainly interested in

the propagating modes. The methods used to compute these modes are outlined in our previous work [11, 15].

For ease of identifying the coupled, the pure elastic and the pure fluid systems to be discussed in the following sections, we use a modal label to represent a particular mode. For instance, P10C, P10A, and P10F mean the propagating (non-evanescent) mode, mode 1 and $n = 0$. The labels C, A, and F represent the "coupled" mode, the pure "annular" cylinder mode and the pure "fluid" mode respectively.

5. STEEL TUBE VIBRATION IN THE AXIALLY SYMMETRIC MODE

5.1. WATER-FILLED STEEL TUBE FOR $n = 0$

First, the axially symmetric waves in the water–steel coupled system with thermal effect are examined. The system matrix is 9×9 as shown in Case 2 in Table 2. In this coupled system, two modes start at the dimensionless frequency $\Omega \approx 0$ as shown in Figure 2. At the beginning (near the zero frequency), the dimensionless phase velocities of modes P10C and P20C in Figure 3(a) are 0·869 (1287 m/s) and 3·43 (5080 m/s) respectively. The wave speed of the first mode P10C is similar to the intrinsic longitudinal plane-wave speed in water and the wave speed of the second mode P20C is similar to the longitudinal wave speed in a bar [2].

As the frequency increases from zero, the first coupled mode, P10C, closely follows the first pure fluid mode P10F (plane wave, first dashed line in Figure 2(a)) and the second mode, P20C, closely follows the first pure elastic wave P10A. Because the first pure elastic mode P10A vibrates longitudinally near zero frequency (Figure 4(a), $\Omega = 0{\cdot}06$), the fluid column and the elastic tube are largely uncoupled. Thus, the mode shape of the first coupled mode P10C (Figure 5(a), $\Omega = 0{\cdot}06$) near zero frequency is similar to the first pure fluid mode P10F (Figure 4(c), at $\Omega = 0{\cdot}06$) and the second coupled mode P20C (Figure 5(b), $\Omega = 0{\cdot}06$) is similar to the first pure elastic mode P10A (Figure 4(a), $\Omega = 0{\cdot}06$). As the frequency increases, the axial phase speed of the first coupled mode P10C decreases as shown in Figure 3(a). This reduction in phase velocity was also observed by Lin and Morgan [5] as mentioned in section 1.

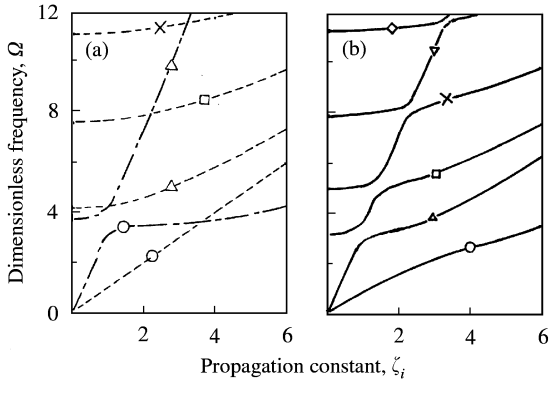

Figure 2. Dispersion curves for water alone, elastic steel tube alone and water–steel coupled systems for $n = 0$ with thermal effect included. The fluid and the elastic systems are largely coupled in lower frequencies: - - - -, fluid alone; – · –, elastic alone; ——, coupled; - -○- -, P10F; - -△- -, P20F; - -□- -, P30F; - - × - -, P40F; – · ○ –, P10A; – · △ –, P20A; –○–, P10C; –△–, P20C; –□–, P30C; – × –, P40C; –▽–, P50C; –◇–, P60C. (a) Uncoupled system; and (b) coupled system.

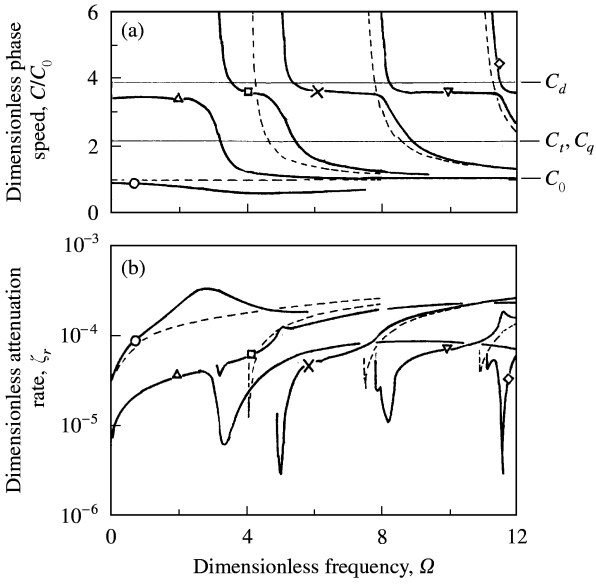

Figure 3. Phase speeds and attenuation rates in a water-filled tube for $n = 0$ with thermal effect included. The second mode P20C has a coincidence frequency at $\Omega = 3{\cdot}35$. The pure fluid modes P10F, P20F, P30F and P40F (dashed lines in sequence) are plotted for helping to understand modal activities of the coupled modes: - - - -, fluid alone; ——, coupled. –○–, P10C; –△–, P20C; –□–, P30C; – × –, P40C; –▽–, P50C; –◇–, P60C. (a) Phase speeds; and (b) attenuation rates.

With increasing frequency, the wave phase speed of the first pure elastic mode P10A reduces and the tube vibrates radially as shown in the 3-D mode-shape plot in Figure 4(a). The frequency-dependent wave speed of the pure elastic mode P10A is similar to the coupled mode P10C in Figure 3(a). When the wave speed in the fluid column and elastic tube are about the same (near the intersection between P10A and P10F in Figure 2(a), at $\Omega = 3{\cdot}35$ (17 764 Hz), the tube and the fluid-column motions become *very* strongly coupled. This phenomenon is called the "coincidence" of the fluid column and the elastic tube, and represents fluid–elastic resonance. At coincidence, the attenuation rate of the coupled mode P20C (elastic-like mode) is significantly reduced by about 10 times, as shown in Figure 3(b).

The coincidence frequency can be roughly estimated from the uncoupled system [2] by equating the axial wave speed of the fluid column to the axial wave speed of the elastic tube in the uncoupled system. By using this method, the *approximate* coincidence was estimated as 3·61, which is about 8%, overestimated from the *actual* coupled coincidence frequency $\Omega_{coincidence} = 3{\cdot}35$, which was found directly from the coupled mode P20C by locating the local minimum of the log-plot (Figure 3(b)) of the attenuation rate versus frequency. In water, the thermal effect does not change the coincidence frequency either in the uncoupled system or the coupled system. Note that not all dips of attenuation rates in the plot are caused by the coincidence phenomenon. For instance, in the fluid-alone system, the attenuation-rate curves dip when the pure fluid modes emerge at cut-off frequencies [10].

Above the coincidence frequency, the wave characteristic of the first two coupled modes are swapped; the first coupled mode P10C now approaches the pure elastic mode P10A and the second mode P20C approaches the second pure fluid mode P20F as shown in Figure 2. Interestingly, the second coupled mode P20C approaches the second pure fluid mode P20F, and *not* the first pure fluid mode P10F since the wave front of the fluid portion of the coupled mode P20C is not flat (or not plane) at $\Omega = 5$ in Figure 5(b). The first pure fluid

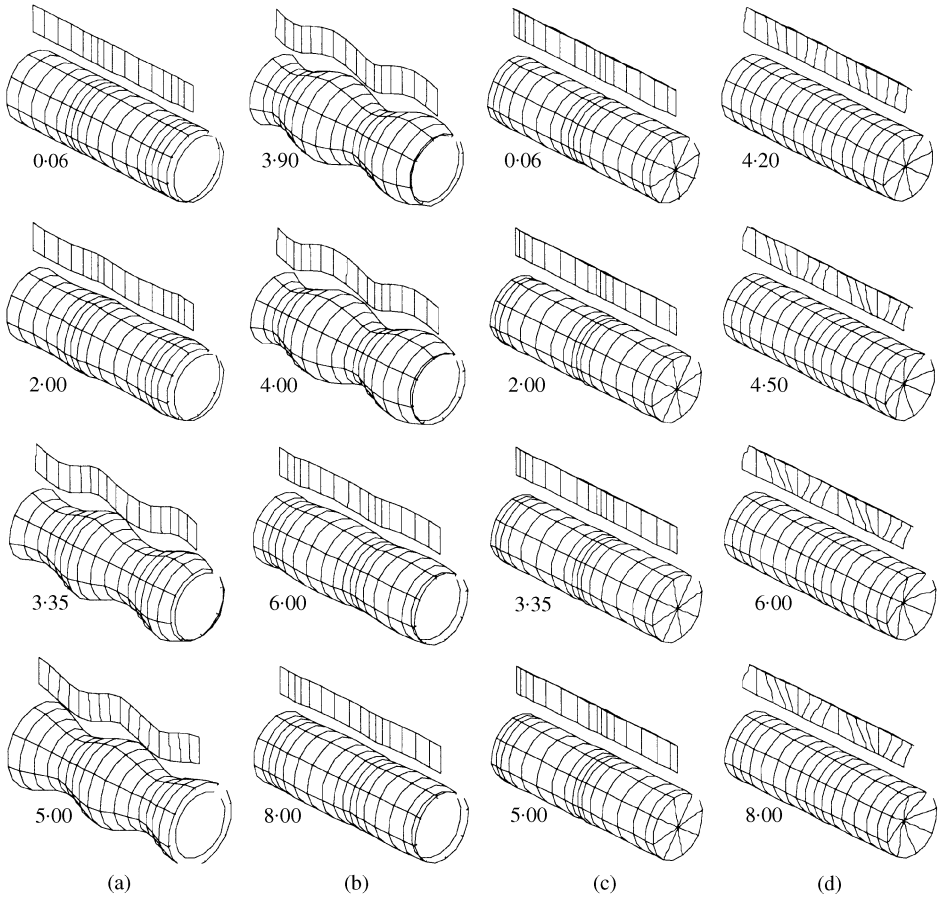

Figure 4. Two/three-dimensional mode shapes of the pure elastic waves and pure fluid waves in the *uncoupled* system for $n = 0$ with thermal effect included. (a) First pure elastic mode P10A at $\Omega = 0{\cdot}06$, 2, 3·35, 5; (b) second pure elastic mode P20A at $\Omega = 3{\cdot}9$, 4, 6, 8; (c) first pure fluid mode P10F at $\Omega = 0{\cdot}06$, 2, 3·35, 5; and (d) second pure fluid mode P20F at $\Omega = 4{\cdot}2$, 4·5, 6, 8.

mode P10F is a plane wave in the range of frequencies studied, while the fluid second mode P20F is not. The fluid column vibration of the coupled mode P10C gradually changes from a longitudinal plane wave to a surface wave as shown in Figure 5(a) (the grid lines in the fluid column are bent near the elastic–fluid interface). The dimensionless phase velocity of mode P10C is 0·606 (897 m/s) at $\Omega = 5$ as shown in Figure 3(a). For a strongly coupled system such as a water-steel system, the longitudinal plane waves of mode P10C (Figure 5(a) in the fluid column exist only near the zero frequency (not all frequencies).

In Figure 3(b), when the frequency increases, the attenuation rate (ζ_r) of the first coupled mode P10C increases at a faster rate than the pure fluid mode P10F and at $\Omega = 2{\cdot}9$ reaches a peak (2·2 times of ζ_r for P10F). A close examination of the 2-D mode-shape plot of the coupled mode P10C in Figure 5(a) at $\Omega = 2{\cdot}9$ shows that the grid lines of the fluid column and the grid lines of the elastic tube do not mesh well, while the second coupled mode P20C meshes very well as shown in Figure 5(b) at $\Omega = 3{\cdot}35$. Therefore, the coupled mode P10C at near-coincidence frequency cannot create "coincidence" but creates a "strong friction-like" effect (i.e., larger relative z direction motion near the elastic–fluid interface). This strong friction could be the cause of the higher attenuation rate as shown in Figure 3(b), mode

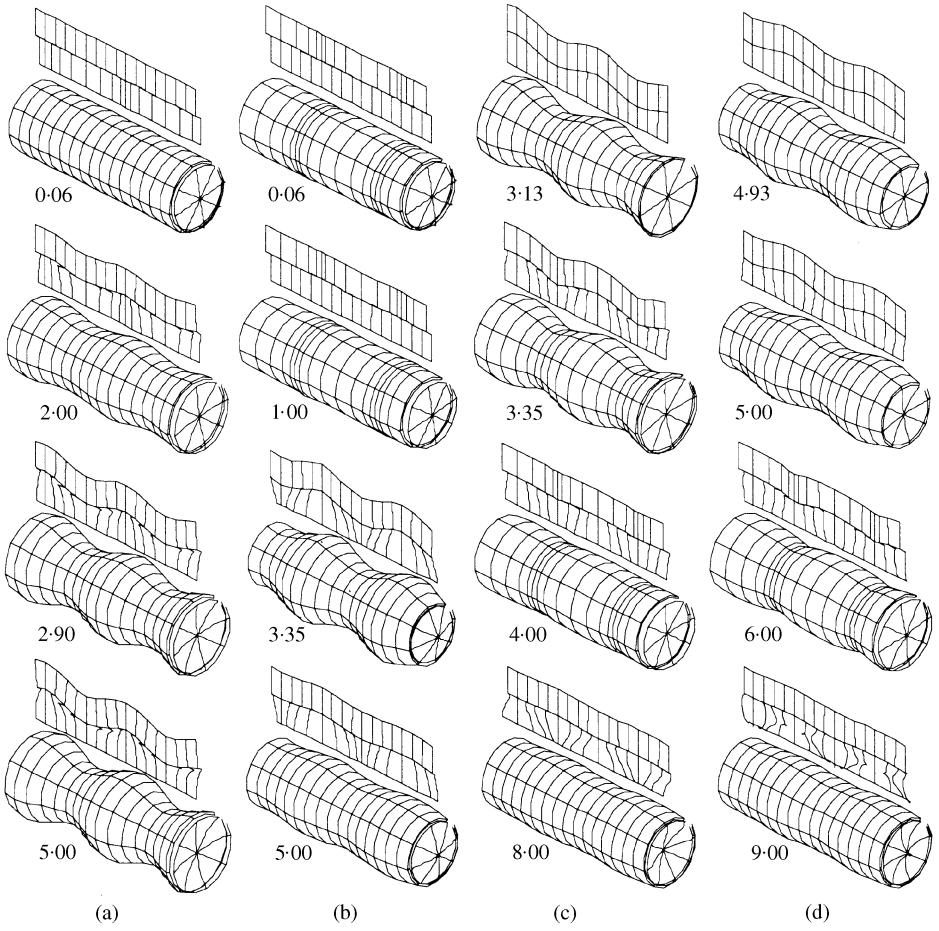

Figure 5. Coupled two/three-dimensional mode shapes of the water-filled tube for $n = 0$ with thermal effect included. The thickness of the elastic portion is magnified. (a) Mode P10C at $\Omega = 0{\cdot}06$, 2, 2·9, 5; (b) mode P20C at $\Omega = 0{\cdot}06$, 1, 3·35, 5; (c) mode P30C at $\Omega = 3{\cdot}13$, 3·35, 4, 8; and (d) mode P40C at $\Omega = 4{\cdot}93$, 5, 6, 9.

P10C. The second coupled mode P20C in Figure 3(b) has the least attenuation rate until the fourth mode takes place at the cut-off frequency, $\Omega = 4{\cdot}93$ (26 143 Hz), where the fourth mode takes over and becomes the least-attenuated mode. The modes P10C and P30C never become the least attenuated mode, thus having little importance for noise control engineers.

The third coupled mode, P30C in Figure 2, emerges at the cut-off frequency $\Omega = 3{\cdot}14$. This coupled mode emerges as an elastic-like mode and follows the pure elastic mode P20A, until the frequency $\Omega = 4{\cdot}93$, then turns sharply approaching the second pure fluid mode P20F. Near this frequency, a fourth mode, P40C, emerges as a fluid-like mode and then changes its behavior to that of an elastic-like mode P20A largely uncoupled from the fluid column (Figure 5(d), $\Omega = 6$), until the frequency $\Omega = 7{\cdot}86$, then turns sharply following the third pure fluid mode P30F. Similarly, with increasing frequency all higher modes emerge as fluid waves, then quickly change their behavior to that of elastic waves, and finally change to the next higher fluid wave. The coupled modes at the fifth and higher modes are nearly uncoupled between the elastic tube and the fluid column due to the fact that the second pure elastic mode, P20A, vibrates longitudinally in higher frequencies as shown in Figure 4(b).

Upon close examination of the log-plot of the attenuation rates in Figure 3(b), the first coupled mode P10C (solid line) near the cut-off frequency is seen to be similar to the first pure fluid mode P10F (dashed line); P40C is similar to P20F near the cut-off frequency; P50C is similar to P30F; P60C is similar to P40F; and the extra coupled modes P20C and P30C are originated at low frequency from the elastic tube. The dips of the attenuation-rate curves at modes P40C, P50C and P60C in Figure 3(b) are from the fluid-like modes emerging at cut-off frequencies.

A thermal effect may not be important for either the elastic-alone or the fluid-alone systems as discussed in references [9, 10]. Even in the water–steel coupled system, the thermal effect can only slightly increase the attenuation rates (less than 1%) except for those frequencies near cutoff and coincidence. The attenuation is mostly contributed by the viscous fluid. The attenuation rates at cutoff and coincidence frequencies are very small; thus, the attenuation contributed by the thermal effect will not be masked by the attenuation contributed by the viscous fluid. If the thermal effect is not included in the water–steel system equations, then the attenuation rates near those cut-off frequencies can result in 8–90% error as shown in Table 3. The attenuation rate near the coincidence frequency ($\Omega = 3{\cdot}35$) of the mode P20C can result in a 12% error as well. The influence of the thermal effect on the propagation constant (ζ_i) of the water–steel system is negligible ($< 0{\cdot}06\%$).

For a pure elastic system used in this paper, Young's modulus is actually real: a complex modulus of elasticity, has an imaginary part representing "structural or hysteretic" damping; since the hysteretic damping does not exist in the pure elastic system, the attenuation rate should be zero. As a reminder, however, one should not be confused by the high attenuation rate in the evanescent wave mentioned in this paper, which for the pure elastic system is basically from the out-of-phase motions between the elastic stress and the elastic strain in the structural acoustical near field. If the thermal effect had been included in the elastic system equation, then the thermal effect could have generated a slight attenuation through the diffusion term, $\partial_t T$ in equation (1a). The thermal effect in the fluid system could also contribute to the attenuation through the term $\partial_t \rho$ in equation (3) and

TABLE 3

A comparison of the attenuation rates (ζ_r) between the thermal effect solutions and the non-thermal effect solutions for a water-filled tube and $n = 0$. The thermal effect is only important for those frequencies near cut-off and coincidence

	P10C			P20C			P30C	
Freq. Ω	Thermal, $\times 10^{-4}$	No th. (error) $\times 10^{-4}$	Freq. Ω	Thermal, $\times 10^{-4}$	No th. (error) $\times 10^{-4}$	Freq. Ω	Thermal, $\times 10^{-4}$	No th. (error) $\times 10^{-4}$
0·08	0·286	0·0706 (75%)	0·06	0·0615	0·0611 (0·7%)	3·134	0·508	0·0528 (90%)
2	2·11	2·10 (0·5%)	1	0·252	0·250 (0·8%)	3·35	0·467	0·451 (3%)
3	3·45	3·44 (0·3%)	3·35	0·0585	0·0517 (12%)	4	0·570	0·563 (1%)
4	2·23	2·22 (0·5%)	5	0·518	0·517 (0·2%)	8	1·97	1·97 (0%)
	P40C			P50C			P60C	
4·931	0·165	0·103 (38%)	7·856	0·676	0·625 (8%)	11·13	0·507	0·458 (10%)
5	0·0225	0·0146 (35%)	8	0·298	0·295 (1%)	11·2	0·453	0·437 (4%)
6	0·506	0·499 (1%)	9	0·597	0·590 (1%)	11·5	0·348	0·345 (0·9)
9	1·66	1·65 (0·6%)	12	0·602	0·595 (1%)	12	0·602	0·595 (1%)

T in equation (7). Because the thermal effect can contribute to the attenuation rate, the attenuation rate from the thermal effect solution in the fluid–elastic coupled system is always higher than the non-thermal effect solution as shown in Table 3. The thermal effect is significant when the attenuation rate is low such as that in cutoff or coincidence frequencies in Table 3.

5.2. AIR-FILLED STEEL TUBE FOR $n = 0$

An air-filled tube does not have the strong fluid–elastic coupling effect as shown in Figure 6(b), unlike a water-filled tube. Since the air has a much higher specific heat ratio (γ_0) and a lower Prandtl number (P_r) than water, the thermal effect in the air-filled tube system is much more prominent than the water-filled tube. The viscous fluid thermal coupling factor was defined in reference [10, equation (37)] as

$$\delta_j = (\gamma_0 - 1)/[1 + i\omega(P_r/v_0 h_j^2)]. \tag{15}$$

The ratios of the specific heat γ_0 of air and water are 1·402 and 1·004 respectively. The Prandtl numbers of air and water are 0·7088 and 7·52 respectively [10]. For $\gamma_0 = 1$, the thermal effect is zero in equation (15).

If the thermal effect is not included in the air–steel coupled system, then the attenuation rate could be underestimated by at least 32% for fluid-like modes (P10C, P20C and P30C) as shown in Figure 7. Near the cut-off frequencies, the error could be as high as 90% as shown in Table 4. The first coupled mode P10C is completely dominated by the fluid-like mode and results in a 32% error if the thermal effect is not included as shown in Figure 7 and Table 4. For the second coupled mode P20C, the dimensionless frequencies in the range $0{\cdot}03 \leqslant \Omega \leqslant 4$ is completely dominated by the elastic-like mode; there is no difference in the attenuation rates between the thermal and the non-thermal solutions as shown in Table 4. The influence of the thermal effect on the propagation constant (ζ_i) of the air–steel system is less than 1%, except for one mode P40C at the cut-off frequency $\Omega = 7{\cdot}54$ having a 6% error (not shown in Table 4).

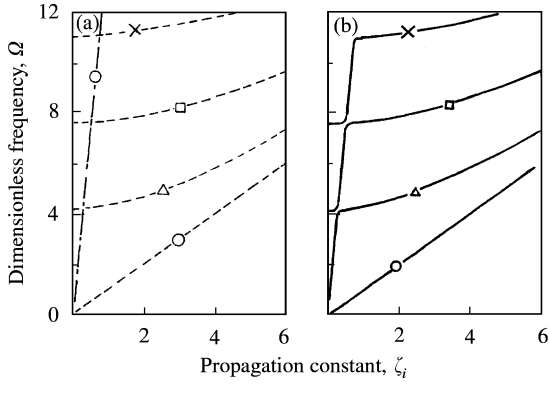

Figure 6. Dispersion curves for air alone, elastic steel tube alone and air–steel coupled systems for $n = 0$ with thermal effect included. The air and the elastic steel tube are nearly uncoupled: ------, fluid alone; –·–, elastic alone; ——, coupled; --○--, P10F; --△--, P20F; --□--, P30F; --×--, P40F; –·○–, P10A; –○–, P10C; –△–, P20C; –□–, P30C; –×–, P40C. (a) Uncoupled system; and (b) coupled system.

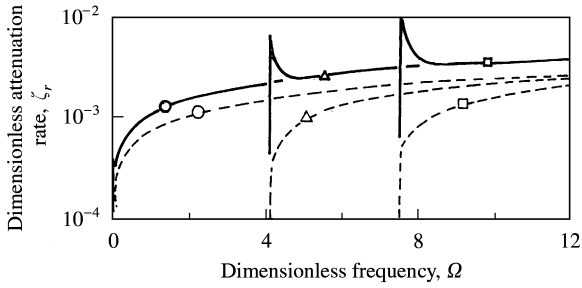

Figure 7. A comparison of attenuation rates between the thermal and non-thermal solutions for an air-filled steel tube, $n = 0$. The attenuation rates from the non-thermal solutions are at least 32% underestimated. The attenuation rates of the coupled mode P20C (— line) in the frequency range 0–4 and the coupled mode P30C in the frequency rate 4–7·5 are nearly zero and are not shown in the plot: —, thermal; - - - -, non-thermal: –○–, P10C; –△–, P20C; –□–, P30C.

TABLE 4

A comparison of the attenuation rates (ζ_r) between the thermal-effect solutions and the non-thermal-effect solutions for an air-filled tube and $n = 0$. The thermal effect can vary the attenuation rates by 32% *or more*

	P10C			P20C			P30C	
Freq. Ω	Thermal, $\times 10^{-4}$	No th. (error) $\times 10^{-4}$	Freq. Ω	Thermal, $\times 10^{-4}$	No th. (error) $\times 10^{-4}$	Freq. Ω	Thermal, $\times 10^{-4}$	No th. (error) $\times 10^{-4}$
0·01	1·12	0·763 (32%)	0·003	0	0 (0%)	4·13	0·0794	0·0053 (93%)
1	11·1	7·54 (32%)	3	0·0009	0·0009 (0%)	6	0·0013	0·0013 (0%)
4	22·5	15·2 (32%)	4·2	42·3	3·68 (91%)	7·6	80·6	5·60 (93%)
12	40·6	27·4 (33%)	12	39·1	25·5 (35%)	12	38·0	0·5 (43%)

6. STEEL TUBE VIBRATION IN THE NON-AXIALLY SYMMETRIC BEAM MODE

6.1. WATER-FILLED TUBE FOR $n = 1$

The system matrix for the non-axially symmetric waves with thermal effect is 12×12 as shown in Case 1 in Table 2 (versus the 9×9 symmetric case). When the tube vibrates non-axially symmetrically, the dispersion curves behave similar to those discussed for the axially symmetric mode ($n = 0$) in section 5. The first coupled mode in the water-filled tube, P11C, follows the first pure elastic mode P11A as shown in Figure 8(b). Near the zero frequency, the phase speed of the non-axially coupled mode P11C is nearly zero, and the attenuation rate is very low as shown in Figure 9. In the first non-axially symmetric mode P11A, the elastic-alone system is a beam-bending mode as shown in the 3-D mode-shape plot in Figure 10(a). This frequency-dependent bending wave speed for P11A (not shown) is seen to be proportional to $\omega^{1/2}$ in low frequencies [2], and then gradually decreases for frequencies $\Omega > 2$. The phase-speed curve of P11A is not plotted, but it is similar to the curve P11C in Figure 9(a).

The second coupled mode, P21C, emerges at $\Omega = 1{\cdot}9$ as a complex mode with a very high attenuation rate, 0·52, until the frequency $\Omega = 2{\cdot}3$, where the attenuation rate drops to 0·00022 and the complex mode changes to the propagating mode. The coupled mode P21C is similar to the first pure fluid mode P11F except near the cut-off frequency.

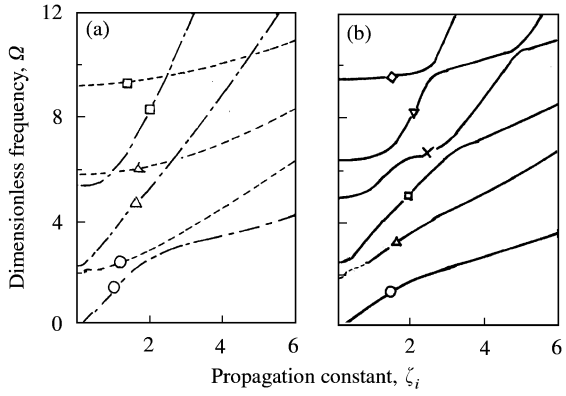

Figure 8. Dispersion curves for water alone, elastic steel tube alone and water–steel coupled systems for $n = 1$ with thermal effect included. The second couple mode P21C in the frequencies 1·9–2·3 is a complex mode (as indicated by the dashed lines): ------, fluid alone; –·–, elastic alone; ——, coupled; --○--, P11F; --△--, P21F; --□--, P31F; –·○–, P11A; –·△–, P21A; –·□–, P31A; –○–, P11C; –△–, P21C; –□–, P31C; –×–, P41C; –▽–, P51C; –◇—, P61C. (a) Uncoupled system; and (b) coupled system.

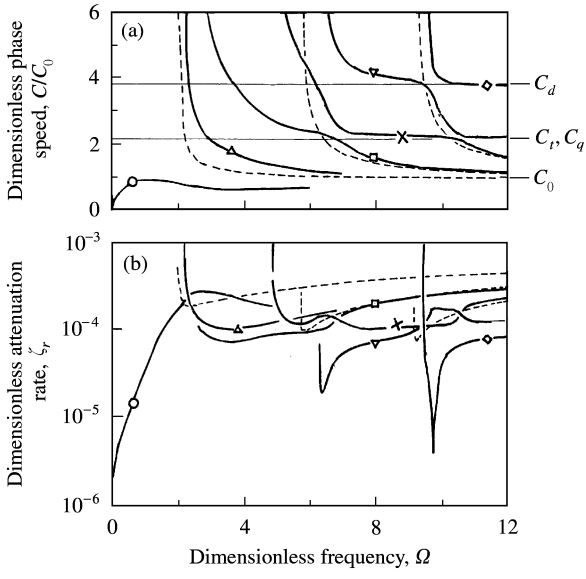

Figure 9. Phase speeds and attenuation rates in a water-filled tube for $n = 1$ with thermal effect included. The pure fluid modes P11F, P21F and P31F (dashed lines in sequence) are plotted for helping to understand modal activities of the coupled modes. The attenuation rates at modes P51C and P61C dip sharply near the cut-off frequencies: ------, fluid alone; ——, coupled. –○–, P11C; –△–, P21C; –□–, P31C; –×–, P41C; –▽–, P51C; –◇–, P61C. (a) Phase speeds; and (b) attenuation rates.

The third coupled mode, P31C, emerges at $\Omega = 2{\cdot}4$. Initially, this mode closely follows the second pure elastic mode P21A until at $\Omega = 6{\cdot}3$, then turns to follow the second fluid mode P21$\bar{\text{H}}$. The fourth coupled mode, P41C, emerges at $\Omega = 4{\cdot}83$, initially following the third pure elastic mode P31A. Later, this mode follows the second pure elastic mode and then the third pure fluid mode at $\Omega = 7{\cdot}0$ and $10{\cdot}5$ respectively. In the frequency range $7 < \Omega < 10{\cdot}5$, the coupled mode P41C vibrates torsionally, as shown in Figure 11(d), at $\Omega = 9$ and its

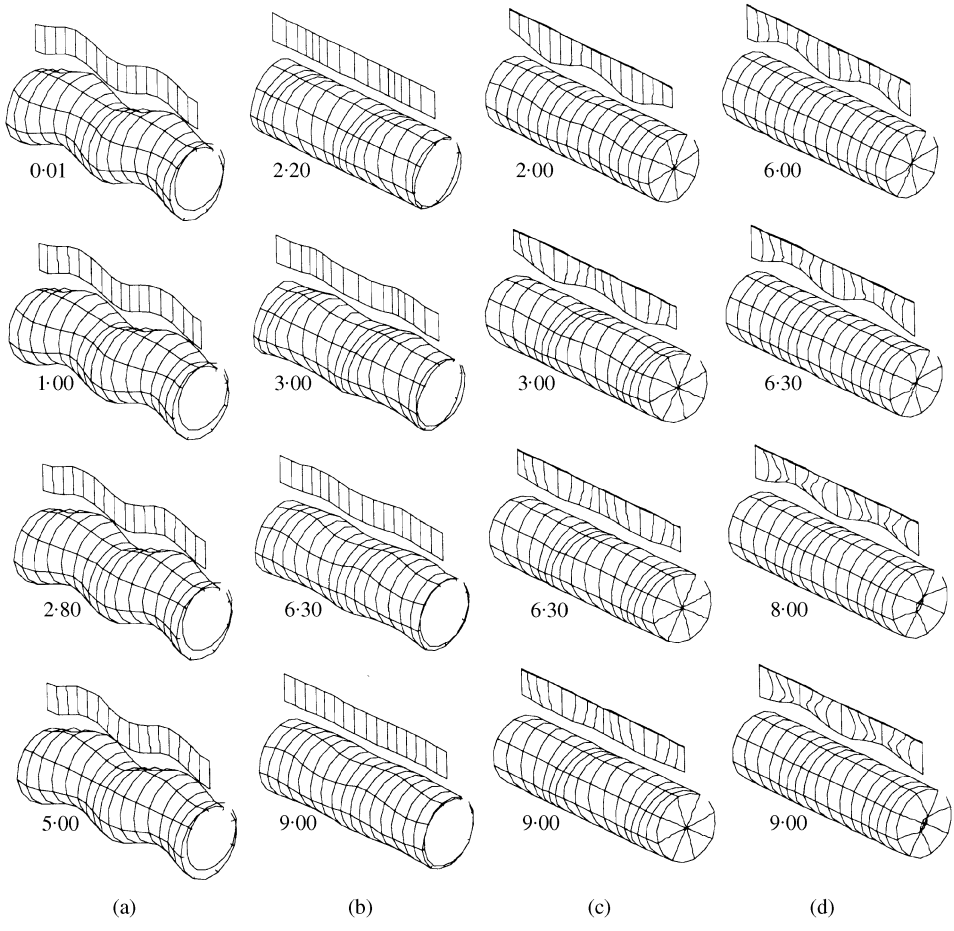

Figure 10. Two/three-dimensional mode shapes of the pure elastic waves and pure fluid waves in the *uncoupled* system for $n = 1$ with thermal effect included. (a) First pure elastic mode P11A at $\Omega = 0{\cdot}01$, 1, 2·8, 5; (b) second pure elastic mode P21A at $\Omega = 2{\cdot}2$, 3, 6·3, 9; (c) first pure fluid mode P11F at $\Omega = 2$, 3, 6·3, 9; and (d) second pure fluid mode P21F at $\Omega = 6$, 6·3, 8, 9.

wave speed is 2·2 (i.e., 3258 m/s) in Figure 9(a). With further increases in frequency, the second pure elastic mode (P21A in Figure 10(b)) becomes a torsional mode, and the third pure elastic mode (P31A not shown in Figure 10) transforms to longitudinal vibration.

The fifth and the sixth coupled modes, P51C and P61C, initially follow the second and third pure fluid modes (P21F and P31F in Figure 8(a)) and obtain the attenuation dips as shown in Figure 9(b). A close examination of the log-plot of the attenuation rates in Figure 9(b) shows that initially, the second coupled mode P21C (solid line) is similar to P11F; P51 C is similar to P21F; and P61C is similar to P31F. Three extra coupled modes, P11C, P31C and P41C, originate for low frequencies from the elastic tube. Interestingly, if the coupled modes initially come from the fluid system such as P51C and P61C, then the attenuation rates will dip sharply near the cut-off frequencies as shown in Figure 9(b).

None of the non-axially symmetric modes in the water-filled tube coupled system have a "strong" coincidence phenomenon in which the attenuation rate drops significantly. The dips in modes P51C and P61C are from the fluid-like mode emergence near the cut-off

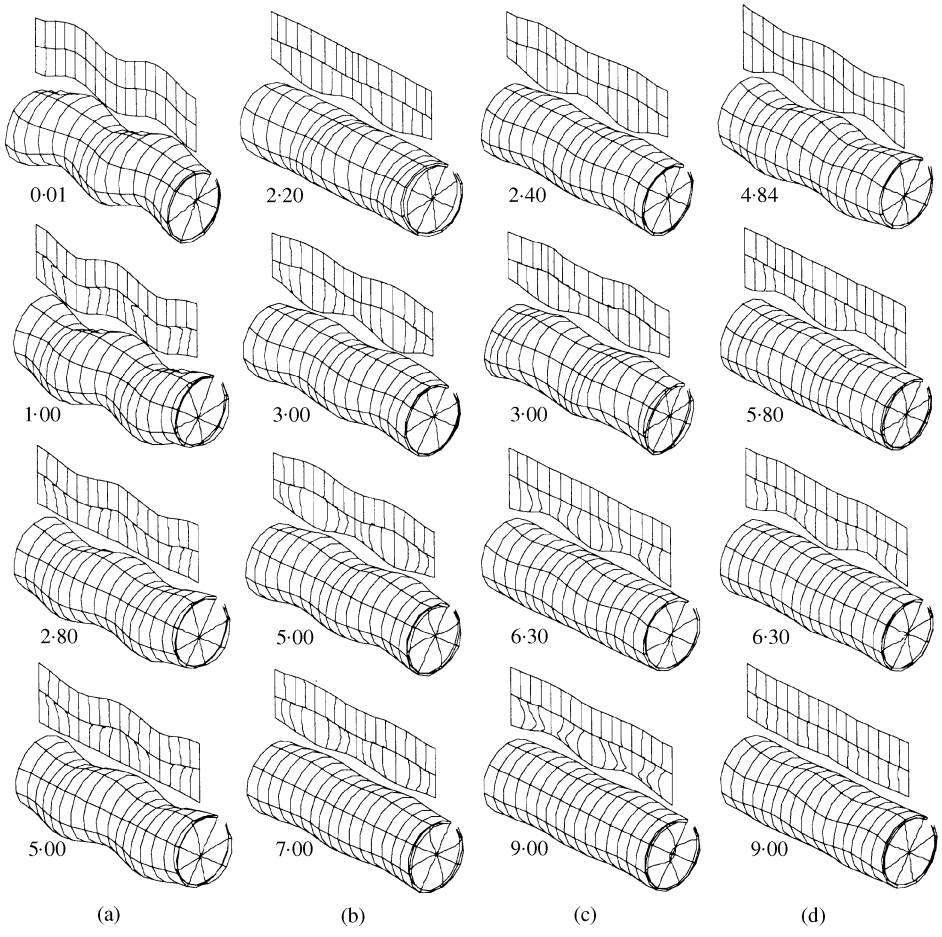

Figure 11. Coupled two/three-dimensional mode shapes of the water-filled tube for $n = 1$ with thermal effect included. The thickness of the elastic part is magnified. (a) Mode P11C at $\Omega = 0{\cdot}01$, 1, 2·8, 5; (b) mode P21C at $\Omega = 2{\cdot}2$, 3, 5, 7; (c) mode P31C at $\Omega = 2{\cdot}4$, 3, 6·3, 9; and (d) mode P41C at $\Omega = 4{\cdot}84$, 5·8, 6·3, 9.

frequencies. Since the second and third pure elastic modes, P21A (Figure 10(b)) and P31A (not shown in Figure 10), are torsional and longitudinal in higher frequencies, the elastic tube lacking the lateral vibration (only generating in these frequencies torsional waves vibrating tangentially, shearing the fluid and only generating viscous induced, and relatively unimportant diffusion waves) cannot excite the fluid portion; thus, the coupled system will not create the coincidence phenomenon. The first pure elastic mode P11A vibrates laterally as shown in Figure 10(a). Since no pure fluid mode intersects with this pure elastic mode as shown in Figure 8(a), no coincidence occurs.

Generally speaking, the non-axially symmetric modes ($n = 1$) of the water–steel coupled system have a lower thermal effect (less than 1%) than the axially symmetric modes ($n = 0$), because the non-axially symmetric modes have relatively higher attenuation rates. However, if the thermal effect is not included in the system equations, then the first mode, P11C, is computed to be 48% in error for Ω near the zero frequency as shown in Table 5; P51C and P61C have 3% and 4% errors, respectively, near the cut-off frequencies.

TABLE 5

A comparison of the attenuation rates (ζ_r) between the thermal-effect solutions and the non-thermal-effect solutions for a water-filled tube and $n = 1$

	P11C			P21C			P31C	
Freq. Ω	Thermal, $\times 10^{-4}$	No th. (error) $\times 10^{-4}$	Freq. Ω	Thermal, $\times 10^{-4}$	No th. (error) $\times 10^{-4}$	Freq. Ω	Thermal, $\times 10^{-4}$	No th. (error) $\times 10^{-4}$
0·01	0·0033	0·0017 (48%)	2·2	11·5	11·5 (0%)	2·4	3·22	3·21 (0·3%)
1	0·276	0·272 (1%)	3	1·05	1·05 (0%)	4	0·735	0·735 (0%)
2·8	2·95	2·95 (0%)	5	1·19	1·19 (0%)	6·3	0·964	0·963 (0·1%)
5	1·80	1·77 (2%)	7	1·59	1·58 (0·6%)	9	2·25	2·24 (0·4%)
	P41C			P51C			P61C	
4·84	52·9	52·3 (1%)	6·349	1·25	1·21 (3%)	9·427	2·15	2·06 (4%)
5·8	1·10	1·09 (0·9%)	9·5	1·15	1·14 (0·9%)	9·76	0·0214	0·0212 (0·9%)
6·3	1·45	1·45 (0%)	10·3	1·69	1·68 (0·6%)	10·3	0·599	0·592 (1%)
9	1·08	1·08 (0%)	11	1·20	1·20 (0%)	11	0·736	0·728 (1%)

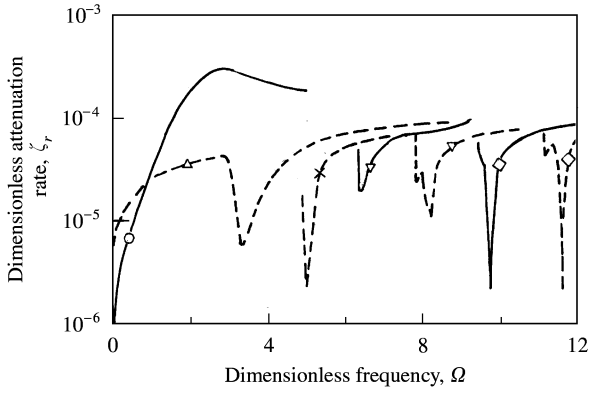

Figure 12. Least attenuated modes in a water-filled tube for $n = 0$, 1 (thermal effect included). The first two least-attenuated modes, P11C and P20C are the elastic-like modes and the rest modes are fluid-like modes: - - - - - -, $n = 0$; ——, $n = 1$. Four axially symmetric modes are: - -△- -, P20C; - - × - -, P40C; - -▽- -, P50C; - -◇- -, P60C. Three non-axially symmetric modes are: –○–, P11C; –▽–, P51C; –◇–, P61C.

For the noise radiation from a water-filled pipeline (transmission loss of the pipe wall), one would be interested in the least-attenuated modes in the elastic pipe. Figure 12 shows the least-attenuated modes for $n = 0$ (axially symmetric modes) and $n = 1$ (non-axially symmetric modes) by overlapping Figures 3(b) and 9(b). The first two least-attenuated modes P11C and P20C originate from the elastic-like modes and will most certainly be an important source of noise radiation of a pipeline in the frequencies less than 4 (i.e., 21 211 Hz). When $\Omega < 1$ (i.e., 5303 Hz), the least-attenuated mode is P11C (beam-bending mode). As $\Omega > 1$, the least-attenuated mode switched to P20C (longitudinal mode in low frequencies). At $\Omega = 3{\cdot}35$ (i.e., 17 764 Hz), the mode P20C vibrates radially and creates a coincidence dip of the attenuation constant as shown in Figure 12. The attenuation constant dips in $\Omega > 4$ are from the emergence of the fluid-like modes.

6.2. AIR-FILLED TUBE FOR $n = 1$

Examining the non-axially symmetric waves for a steel pipe containing air indicated that the coupling effect and the thermal effect are very similar to the axially symmetric waves. The study of the first coupled mode P11C of the air-filled tube system reveals a similar behavior with a 35–40% error if the thermal effect is not included in the dimensionless frequency range $3 \leqslant \Omega \leqslant 5$.

7. CONCLUSIONS

In a water-filled tube, a coincidence phenomenon occurred in the second coupled mode P20C for $n = 0$ at $\Omega = 3{\cdot}35$ (17 764 Hz), where the fluid and elastic wave speed are the same; the fluid column and the elastic wall are in resonance. When coincidence occurs, the tube vibrates radially and the vibrational axial displacements near the elastic–fluid interface naturally meshes so that a strong coupling is easily achieved due to the lack of severe spatial gradients at the satisfied interfacial boundary conditions. The "coincidence" for the fully coupled system will cause the attenuation rate to drop substantially. No "strong" coincidence was found for $n = 1$ in the frequency range considered even though there were several possible intersections between the purely elastic modes and the purely fluid modes in Figure 8(a). In the low frequencies, the dispersion curves of the water–steel coupled system were considerably different from the uncoupled system. For frequencies above $\Omega = 8$, the water column and the elastic tube were largely uncoupled in the $n = 0$ and 1 cases.

For the air–steel coupled system, the fluid and the elastic systems were largely uncoupled for the entire frequency range. However, the *thermal* effect in the air–steel system was very prominent. In the $n = 0$ case, the modal attenuation rates of the air–steel system could be underestimated by at least 32% for the entire first mode if the thermal effect is not included, since the thermal effect provides additional attenuation.

REFERENCES

1. M. PAIDOUSSIS *Fluid–Structure Interactions*, Vol. 2. London: Academic Press. (to be published).
2. F. J. FAHY 1985 *Sound and Structural Vibration*. San Diego: Academic Press Ltd, p. 10, 23 and 208.
3. H. LAMB 1898 *Manchester Literary and Philosophical Society—Memoirs and Proceedings*, Vol. 42. On the velocity of sound in a tube, as affected by the elasticity of the walls.
4. W. T. Thomson 1951 *Proceedings of the First U.S. National Congress on Applied Mechanics* 927–933. Transmission of pressure waves in liquid tubes.
5. T. C. LIN and G. W. MORGAN 1956 *The Journal of the Acoustical Society of America* **28**, 1165–1176. Wave propagation through fluid contained in a cylinder, elastic shell.
6. R. KUMAR 1972 *Acustica* **27**, 317–329. Dispersion of axially symmetric waves in empty and fluid-filled cylindrical shells.
7. C. R. FULLER and F. J. FAHY 1982 *Journal of Sound and Vibration* **81**, 501–518. Characteristics of wave propagation and energy distributions in cylindrical elastic shells filled with fluid.
8. C. M. CHANG, W. C. KENNEDY and H. A. SCARTON 1987 *ASME Winter Annual Meeting*, 13–23; ASME paper number 87-WA/NCA-1. Propagation of nonaxisymmetric coincidence modes in a liquid-filled circular cylindrical pipe having a linearly elastic wall of finite thickness.
9. P. N. LIANG and H. A. SCARTON 1994 *Journal of Sound and Vibration* **177**, 121–135. Three-dimensional mode shapes for higher order circumferential thermoelastic waves in an annular elastic cylinder.
10. P. N. LIANG and H. A. SCARTON 1996 *Journal of Sound and Vibration* **193**, 1099–1113. Attenuation of higher order circumferential thermoacoustic waves in viscous fluid lines.
11. P. N. LIANG 1990 *Ph.D. Thesis*, *Rensselaer Polytechnic Institute*. Thermoacoustic wave propagation within a slightly compressible viscous fluid-filled impermeable cylindrical elastic tube. See sections 2.4 and 4.4–4.6 (UMI 91-11065).

12. H. A. SCARTON and W. T. ROULEAU 1973 *Journal of Fluid Mechanics* **58** (Part 3), 595–621. Axisymmetric waves in compressible Newtonian liquids contained in rigid tubes: steady-periodic mode shape and dispersion by the method of eigenvalleys.
13. L. CREMER, M. HECKL and E. E. UNGAR 1988 *Structural-Borne Sound*, p. 93. Berlin, Heidelberg: Springer-Verlag; second edition.
14. W. F. ALBERS, E. J. BRUNELLE and H. A. SCARTON 1985 *Transactions of the American Society of Mechanical Engineers, Journal of Vibration, Acoustics, Stress, and Reliability in Design* **107**, 243–252. The application of a biorthogonality principle to the solution of the end problem of a liquid-filled rectangular viscous acoustic waveguide.
15. H. A. SCARTON 1973 *Journal of Computational Physics* **11**, 1–4. The method of eigenvalleys.

APPENDIX A: ELEMENTS OF MATRIX **D**

From the error analysis [11], the error of the eigenvalues can be reduced if we can improve the matrix (i.e., reduce the condition number of determinant D_{jk}) by properly scaling the system matrix. From experience (based on the concept of minimum condition number), there are three columns in the matrix **D** that need to be scaled as follows:

$$\frac{\zeta}{\Omega^2}\{D_{j,6}\} = \left\{\frac{\zeta}{\Omega^2} D_{j,6}\right\}, \quad \frac{\zeta}{\Omega^2}\{D_{j,8}\} = \left\{\frac{\zeta}{\Omega^2} D_{j,8}\right\}, \quad \frac{D_0\zeta}{i\Omega}\{D_{j,12}\} = \left\{\frac{D_0\zeta}{i\Omega} D_{j,12}\right\}, \quad j = 1\text{–}12.$$

Three new dimensionless wave speeds (dilatational, transverse and torsional) are defined by normalizing each of them, respectively, with the much lower fluid wave speed C_0: $C_D = C_d/C_0$, $C_T = C_t/C_0$ and $C_Q = C_q/C_0$ (C_Q is defined for completeness, but is not used in this Appendix).

These additional normalizations were unnecessary in our fluid column paper [10], and were quite different for our elastic cylindrical annulus paper [9]. The fluid unbounded speed was selected so that most of the dimensionless wave speeds would be larger than 1, the dimensionless unbounded fluid wave speed. This selection greatly aided the interpretation of the dominant mechanisms.

Some dimensionless parameters are defined as follows for the elastic–fluid coupled system:

$$\zeta = ka, \quad \Omega = \frac{\omega a}{C_0}, \quad D_0 = \frac{v_0}{C_0 a}, \quad D_0' = \frac{v_0'}{C_0 a},$$

$$Z_1 = \alpha_1 a, \quad Z_2 = \alpha_2 a, \quad Z_3 = \beta a, \quad W_1 = \gamma_1 a, \quad W_2 = \gamma_2 a, \quad W_3 = \lambda a,$$

$$\Gamma_1 = h_1 a, \quad \Gamma_2 = h_2 a, \quad \mathbb{R} = \frac{b}{a} = 0{\cdot}93138,$$

$$K^* = \frac{k_f}{k_s}, \quad \hbar = \frac{h_f a}{k_s}, \quad G^* = \frac{v_0 \rho_0 C_t}{a\mu}, \quad T^* = m\left\{\frac{P_r C_0 C_t a}{v_0}\left[\frac{T_0}{(\gamma_0 - 1)c_p}\right]^{1/2}\right\}.$$

The elements of the **D** matrix are

$$D_{1,1} = (n^2 - n - \zeta^2 R^2 - \tfrac{1}{2} R^2 \Omega^2 / C_T^2) J_n(Z_1 R) + Z_1 R J_{n+1}(Z_1 R), \; R = 1,$$

$$D_{1,2} = (n^2 - n - \zeta^2 R^2 - \tfrac{1}{2} R^2 \Omega^2 / C_T^2) Y_n(Z_1 R) + Z_1 R Y_{n+1}(Z_1 R), \; R = 1,$$

$$D_{1,3} = (n^2 - n - \zeta^2 R^2 - \tfrac{1}{2} R^2 \Omega^2 / C_T^2) J_n(Z_2 R) + Z_2 R J_{n+1}(Z_2 R),\ R = 1,$$

$$D_{1,4} = (n^2 - n - \zeta^2 R^2 - \tfrac{1}{2} R^2 \Omega^2 / C_T^2) K_n(\mathrm{i} Z_2 R) + Z_2 R \mathrm{i} K_{n+1}(\mathrm{i} Z_2 R),\ R = 1,$$

$$D_{1,5} = \zeta \left[\frac{1}{Z_3} (n^2 - n - Z_3^2 R^2) J_n(Z_3 R) + R J_{n+1}(Z_3 R) \right],\ R = 1,$$

$$D_{1,6} = \frac{1}{Z_3} (n^2 - n) J_n(Z_3 R) - n R J_{n+1}(Z_3 R),\ R = 1,$$

$$D_{1,7} = \zeta \left[\frac{1}{Z_3} (n^2 - n - Z_3^2 R^2) Y_n(Z_3 R) + R Y_{n+1}(Z_3 R) \right],\ R = 1,$$

$$D_{1,8} = \frac{1}{Z_3} (n^2 - n) Y_n(Z_3 R) - n R Y_{n+1}(Z_3 R),\ R = 1,$$

$$D_{1,9} = D_{1,10} = D_{1,11} = D_{1,12} = 0,$$

$$D_{2,1} = 2\zeta [n J_n(Z_1 R) - Z_1 R J_{n+1}(Z_1 R)],\ R = 1,$$

$$D_{2,2} = 2\zeta [n Y_n(Z_1 R) - Z_1 R Y_{n+1}(Z_1 R)],\ R = 1,$$

$$D_{2,3} = 2\zeta [n J_n(Z_2 R) - Z_2 R J_{n+1}(Z_2 R)],\ R = 1,$$

$$D_{2,4} = 2\zeta [n K_n(\mathrm{i} Z_2 R) - Z_2 R \mathrm{i} K_{n+1}(\mathrm{i} Z_2 R)],\ R = 1,$$

$$D_{2,5} = (\zeta^2 + Z_3^2) \left[\frac{n}{Z_3} J_n(Z_3 R) - R J_{n+1}(Z_3 R) \right],\ R = 1,$$

$$D_{2,6} = \zeta \frac{n}{Z_3} J_n(Z_3 R),\ R = 1,$$

$$D_{2,7} = (\zeta^2 + Z_3^2) \left[\frac{n}{Z_3} Y_n(Z_3 R) - R Y_{n+1}(Z_3 R) \right],\ R = 1,$$

$$D_{2,8} = \zeta \frac{n}{Z_3} Y_n(Z_3 R),\ R = 1,$$

$$D_{2,9} = D_{2,10} = D_{2,11} = D_{2,12} = 0,$$

$$D_{3,1} = (n^2 - n) J_n(Z_1 R) - n Z_1 R J_{n+1}(Z_1 R),\ R = 1,$$

$$D_{3,2} = (n^2 - n) Y_n(Z_1 R) - n Z_1 R Y_{n+1}(Z_1 R),\ R = 1,$$

$$D_{3,3} = (n^2 - n) J_n(Z_2 R) - n Z_2 R J_{n+1}(Z_2 R),\ R = 1,$$

$$D_{3,4} = (n^2 - n)K_n(\mathrm{i}Z_2R) - nZ_2R\mathrm{i}K_{n+1}(\mathrm{i}Z_2R),\ R = 1,$$

$$D_{3,5} = \frac{\zeta}{Z_3}(n^2 - n)J_n(Z_3R) - n\zeta RJ_{n+1}(Z_3R),\ R = 1,$$

$$D_{3,6} = \frac{1}{Z_3}(n^2 - n - \tfrac{1}{2}Z_3^2R^2)J_n(Z_3R) + RJ_{n+1}(Z_3R),\ R = 1,$$

$$D_{3,7} = \frac{\zeta}{Z_3}(n^2 - n)Y_n(Z_3R) - n\zeta RY_{n+1}(Z_3R),\ R = 1,$$

$$D_{3,8} = \frac{1}{Z_3}(n^2 - n - \tfrac{1}{2}Z_3^2R^2)Y_n(Z_3R) + RY_{n+1}(Z_3R),\ R = 1,$$

$$D_{3,9} = D_{3,10} = D_{3,11} = D_{3,12} = 0,$$

$$D_{4,1} = \left(\frac{\Omega^2}{C_D^2} - \Lambda_1^2\right)[(n + \hbar R)J_n(Z_1R) - Z_1RJ_{n+1}(Z_1R)],\ R = 1,$$

$$D_{4,2} = \left(\frac{\Omega^2}{C_D^2} - \Lambda_1^2\right)[(n + \hbar R)Y_n(Z_1R) - Z_1RY_{n+1}(Z_1R)],\ R = 1,$$

$$D_{4,3} = \left(\frac{\Omega^2}{C_D^2} - \Lambda_2^2\right)[(n + \hbar R)J_n(Z_2R) - Z_2RJ_{n+1}(Z_2R)],\ R = 1,$$

$$D_{4,4} = \left(\frac{\Omega^2}{C_D^2} - \Lambda_2^2\right)[(n + \hbar R)K_n(\mathrm{i}Z_2R) - Z_2R\mathrm{i}K_{n+1}(\mathrm{i}Z_2R)],\ R = 1,$$

$$D_{4,5} = D_{4,6} = D_{4,7} = D_{4,8} = D_{4,9} = D_{4,10} = D_{4,11} = D_{4,12} = 0,$$

$$D_{5,1} = (n^2 - n - \zeta^2R^2 - \tfrac{1}{2}R^2\Omega^2/C_T^2)J_n(Z_1R) + Z_1RJ_{n+1}(Z_1R),\ R = \mathbb{R},$$

$$D_{5,2} = (n^2 - n - \zeta^2R^2 - \tfrac{1}{2}R^2\Omega^2/C_T^2)Y_n(Z_1R) + Z_1RY_{n+1}(Z_1R),\ R = \mathbb{R},$$

$$D_{5,3} = (n^2 - n - \zeta^2R^2 - \tfrac{1}{2}R^2\Omega^2/C_T^2)J_n(Z_2R) + Z_2RJ_{n+1}(Z_2R),\ R = \mathbb{R},$$

$$D_{5,4} = (n^2 - n - \zeta^2R^2 - \tfrac{1}{2}R^2\Omega^2/C_T^2)K_n(\mathrm{i}Z_2R) + Z_2R\mathrm{i}K_{n+1}(\mathrm{i}Z_2R),\ R = \mathbb{R},$$

$$D_{5,5} = \zeta\left[\frac{1}{Z_3}(n^2 - n - Z_3^2R^2)J_n(Z_3R) + RJ_{n+1}(Z_3R)\right],\ R = \mathbb{R},$$

$$D_{5,6} = \frac{1}{Z_3}(n^2 - n)J_n(Z_3R) - nRJ_{n+1}(Z_3R),\ R = \mathbb{R},$$

$$D_{5,7} = \zeta\left[\frac{1}{Z_3}(n^2 - n - Z_3^2R^2)\,Y_n(Z_3R) + RY_{n+1}(Z_3R)\right],\ R = \mathbb{R},$$

$$D_{5,8} = \frac{1}{Z_3}(n^2 - n)\,Y_n(Z_3R) - nRY_{n+1}(Z_3R),\ R = \mathbb{R},$$

$$D_{5,9} = -G^*\left\{\left[(1+\delta_1)\left(n^2 - n - W_1^2R^2 - \left(\frac{D_0'}{2D_0} - \frac{1}{3}\right)\Gamma_1^2R^2\right) + \frac{\mathrm{i}}{2D_0\Omega}\Gamma_1^2R^2\right]\right.$$
$$\left.\times J_n(W_1R) + W_1RJ_{n+1}(W_1R)\right\},\ R = \mathbb{R},$$

$$D_{5,10} = -G^*\left\{\left[(1+\delta_2)\left(n^2 - n - W_2^2R^2 - \left(\frac{D_0'}{2D_0} - \frac{1}{3}\right)\Gamma_2^2R^2\right) + \frac{\mathrm{i}}{2D_0\Omega}\Gamma_2^2R^2\right]\right.$$
$$\left.\times J_n(W_2R) + W_2RJ_{n+1}(W_2R)\right\},\ R = \mathbb{R},$$

$$D_{5,11} = -G^*\left\{\frac{\zeta}{W_3}(n^2 - n - W_3^2R^2)J_n(W_3R) + \zeta RJ_{n+1}(W_3R)\right\},\ R = \mathbb{R},$$

$$D_{5,12} = -G^*\left\{\frac{-1}{W_3}(n^2 - n)J_n(W_3R) + nRJ_{n+1}(W_3R)\right\},\ R = \mathbb{R},$$

$$D_{6,1} = 2\zeta\,[nJ_n(Z_1R) - Z_1RJ_{n+1}(Z_1R)],\ R = \mathbb{R},$$

$$D_{6,2} = 2\zeta\,[nY_n(Z_1R) - Z_1RY_{n+1}(Z_1R)],\ R = \mathbb{R},$$

$$D_{6,3} = 2\zeta\,[nJ_n(Z_2R) - Z_2RJ_{n+1}(Z_2R)],\ R = \mathbb{R},$$

$$D_{6,4} = 2\zeta\,[nK_n(\mathrm{i}Z_2R) - Z_2R\mathrm{i}K_{n+1}(\mathrm{i}Z_2R)],\ R = \mathbb{R},$$

$$D_{6,5} = (\zeta^2 + Z_3^2)\left[\frac{n}{Z_3}J_n(Z_3R) - RJ_{n+1}(Z_3R)\right],\ R = \mathbb{R},$$

$$D_{6,6} = \zeta\,\frac{n}{Z_3}\,J_n(Z_3R),\ R = \mathbb{R},$$

$$D_{6,7} = (\zeta^2 + Z_3^2)\left[\frac{n}{Z_3}\,Y_n(Z_3R) - RY_{n+1}(Z_3R)\right],\ R = \mathbb{R},$$

$$D_{6,8} = \zeta\,\frac{n}{Z_3}\,Y_n(Z_3R),\ R = \mathbb{R},$$

$$D_{6,9} = -G^*2\zeta(1+\delta_1)\,[nJ_n(W_1R) - W_1RJ_{n+1}(W_1R)],\ R = \mathbb{R},$$

$$D_{6,10} = -G^*2\zeta(1+\delta_2)[nJ_n(W_2R) - W_2RJ_{n+1}(W_2R)],\ R = \mathbb{R},$$

$$D_{6,11} = -G^*(\zeta^2 + W_3^2)\left[\frac{n}{W_3}J_n(W_3R) - RJ_{n+1}(W_3R)\right],\ R = \mathbb{R},$$

$$D_{6,12} = G^*\zeta\frac{n}{W_3}J_n(W_3R),\ R = \mathbb{R},$$

$$D_{7,1} = (n^2 - n)J_n(Z_1R) - nZ_1RJ_{n+1}(Z_1R),\ R = \mathbb{R},$$

$$D_{7,2} = (n^2 - n)Y_n(Z_1R) - nZ_1RY_{n+1}(Z_1R),\ R = \mathbb{R},$$

$$D_{7,3} = (n^2 - n)J_n(Z_2R) - nZ_2RJ_{n+1}(Z_2R),\ R = \mathbb{R},$$

$$D_{7,4} = (n^2 - n)K_n(\mathrm{i}Z_2R) - nZ_2R\mathrm{i}K_{n+1}(\mathrm{i}Z_2R),\ R = \mathbb{R},$$

$$D_{7,5} = \frac{\zeta}{Z_3}(n^2 - n)J_n(Z_3R) - n\zeta RJ_{n+1}(Z_3R),\ R = \mathbb{R},$$

$$D_{7,6} = \frac{1}{Z_3}(n^2 - n - Z_3^2R^2/2)J_n(Z_3R) + RJ_{n+1}(Z_3R),\ R = \mathbb{R},$$

$$D_{7,7} = \frac{\zeta}{Z_3}(n^2 - n)Y_n(Z_3R) - n\zeta RY_{n+1}(Z_3R),\ R = \mathbb{R},$$

$$D_{7,8} = \frac{1}{Z_3}(n^2 - n - Z_3^2R^2/2)Y_n(Z_3R) + RY_{n+1}(Z_3R),\ R = \mathbb{R},$$

$$D_{7,9} = -G^*n(1+\delta_1)[(n-1)J_n(W_1R) - W_1RJ_{n+1}(W_1R)],\ R = \mathbb{R},$$

$$D_{7,10} = -G^*n(1+\delta_2)[(n-1)J_n(W_2R) - W_2RJ_{n+1}(W_2R)],\ R = \mathbb{R},$$

$$D_{7,11} = -G^*n\zeta[(n-1)J_n(W_3R)/W_3 - RJ_{n+1}(W_3R)],\ R = \mathbb{R},$$

$$D_{7,12} = -G^*\left[\frac{-1}{W_3}(n^2 - n - W_3^2R^2/2)J_n(W_3R) - RJ_{n+1}(W_3R)\right],\ R = \mathbb{R},$$

$$D_{8,1} = nJ_n(Z_1R) - Z_1RJ_{n+1}(Z_1R),\ R = \mathbb{R},$$

$$D_{8,2} = nY_n(Z_1R) - Z_1RY_{n+1}(Z_1R),\ R = \mathbb{R},$$

$$D_{8,3} = nJ_n(Z_2R) - Z_2RJ_{n+1}(Z_2R),\ R = \mathbb{R},$$

$$D_{8,4} = nK_n(\mathrm{i}Z_2R) - Z_2R\mathrm{i}K_{n+1}(\mathrm{i}Z_2R),\ R = \mathbb{R},$$

$$D_{8,5} = \frac{n\zeta}{Z_3} J_n(Z_3R) - \zeta R J_{n+1}(Z_3R),\ R = \mathbb{R},$$

$$D_{8,6} = \frac{n}{Z_3} J_n(Z_3R),\ R = \mathbb{R},$$

$$D_{8,7} = \frac{n\zeta}{Z_3} Y_n(Z_3R) - \zeta R Y_{n+1}(Z_3R),\ R = \mathbb{R},$$

$$D_{8,8} = \frac{n}{Z_3} Y_n(Z_3R),\ R = \mathbb{R},$$

$$D_{8,9} = -(1+\delta_1)[nJ_n(W_1R) - W_1RJ_{n+1}(W_1R)]/(\mathrm{i}\Omega),\ R = \mathbb{R},$$

$$D_{8,10} = -(1+\delta_2)[nJ_n(W_2R) - W_2RJ_{n+1}(W_2R)]/(\mathrm{i}\Omega),\ R = \mathbb{R},$$

$$D_{8,11} = -\left[\frac{n\zeta}{W_3} J_n(W_3R) - \zeta R J_{n+1}(W_3R)\right] \Big/ (\mathrm{i}\Omega),\ R = \mathbb{R},$$

$$D_{8,12} = \frac{n}{W_3} J_n(W_3R)/(\mathrm{i}\Omega),\ R = \mathbb{R},$$

$$D_{9,1} = \zeta J_n(Z_1R),\ R = \mathbb{R}, \quad D_{9,2} = \zeta Y_n(Z_1R),\ R = \mathbb{R},$$

$$D_{9,3} = \zeta J_n(Z_2R),\ R = \mathbb{R}, \quad D_{9,4} = \zeta K_n(\mathrm{i}Z_2R),\ R = \mathbb{R},$$

$$D_{9,5} = Z_3 J_n(Z_3R),\ R = \mathbb{R}, \quad D_{9,7} = Z_3 Y_n(Z_3R),\ R = \mathbb{R},$$

$$D_{9,9} = -(1+\delta_1)\zeta J_n(W_1R)/\mathrm{i}\Omega),\ R = \mathbb{R},$$

$$D_{9,10} = -(1+\delta_2)\zeta J_n(W_2R)/\mathrm{i}\Omega),\ R = \mathbb{R},$$

$$D_{9,11} = -W_3 J_n(W_3R)/(\mathrm{i}\Omega),\ R = \mathbb{R},$$

$$D_{9,6} = D_{9,8} = D_{9,12} = 0,$$

$$D_{10,1} = nJ_n(Z_1R),\ R = \mathbb{R}, \quad D_{10,2} = nY_n(Z_1R),\ R = \mathbb{R},$$

$$D_{10,3} = nJ_n(Z_2R),\ R = \mathbb{R}, \quad D_{10,4} = nK_n(\mathrm{i}Z_2R),\ R = \mathbb{R},$$

$$D_{10,5} = \frac{n\zeta}{Z_3} J_n(Z_3R),\ R = \mathbb{R},$$

$$D_{10,6} = \frac{n}{Z_3} J_n(Z_3R) - RJ_{n+1}(Z_3R),\ R = \mathbb{R},$$

$$D_{10,7} = \frac{n\zeta}{Z_3} Y_n(Z_3R),\ R = \mathbb{R},$$

$$D_{10,8} = \frac{n}{Z_3} Y_n(Z_3R) - RY_{n+1}(Z_3R),\ R = \mathbb{R},$$

$$D_{10,9} = -n(1+\delta_1)J_n(W_1R)/(\mathrm{i}\Omega),\ R = \mathbb{R},$$

$$D_{10,10} = -n(1+\delta_2)J_n(W_2R)/(\mathrm{i}\Omega),\ R = \mathbb{R},$$

$$D_{10,11} = -\frac{n\zeta}{W_3} J_n(W_3R)/(\mathrm{i}\Omega),\ R = \mathbb{R},$$

$$D_{10,12} = \left[\frac{n}{W_3} J_n(W_3R) - RJ_{n+1}(W_3R)\right] \Big/ (\mathrm{i}\Omega),\ R = \mathbb{R},$$

$$D_{11,1} = \left(\frac{\Omega^2}{C_D^2} - \Lambda_1^2\right) J_n(Z_1R),\ R = \mathbb{R}, \quad D_{11,2} = \left(\frac{\Omega^2}{C_D^2} - \Lambda_1^2\right) Y_n(Z_1R),\ R = \mathbb{R},$$

$$D_{11,3} = \left(\frac{\Omega^2}{C_D^2} - \Lambda_2^2\right) J_n(Z_2R),\ R = \mathbb{R}, \quad D_{11,4} = \left(\frac{\Omega^2}{C_D^2} - \Lambda_2^2\right) K_n(\mathrm{i}Z_2R),\ R = \mathbb{R},$$

$$D_{11,9} = -T^*\delta_1 J_n(W_1R),\ R = \mathbb{R},$$

$$D_{11,10} = -T^*\delta_2 J_n(W_2R),\ R = \mathbb{R},$$

$$D_{11,5} = D_{11,6} = D_{11,7} = D_{11,8} = D_{11,11} = D_{11,12} = 0,$$

$$D_{12,1} = \left(\frac{\Omega^2}{C_D^2} - \Lambda_1^2\right)[nJ_n(Z_1R) - Z_1RJ_{n+1}(Z_1R)],\ R = \mathbb{R},$$

$$D_{12,2} = \left(\frac{\Omega^2}{C_D^2} - \Lambda_1^2\right)[nY_n(Z_1R) - Z_1RY_{n+1}(Z_1R)],\ R = \mathbb{R},$$

$$D_{12,3} = \left(\frac{\Omega^2}{C_D^2} - \Lambda_2^2\right)[nJ_n(Z_2R) - Z_2RJ_{n+1}(Z_2R)],\ R = \mathbb{R},$$

$$D_{12,4} = \left(\frac{\Omega^2}{C_D^2} - \Lambda_2^2\right)[nK_n(\mathrm{i}Z_2R) - Z_2R\mathrm{i}K_{n+1}(\mathrm{i}Z_2R)],\ R = \mathbb{R},$$

$$D_{12,9} = -K^*T^*\delta_1[nJ_n(W_1R) - W_1RJ_{n+1}(W_1R)],\ R = \mathbb{R},$$

$$D_{12,10} = -K^*T^*\delta_2[nJ_n(W_2R) - W_2RJ_{n+1}(W_2R)],\ R = \mathbb{R},$$

$$D_{12,5} = D_{12,6} = D_{12,7} = D_{12,8} = D_{12,11} = D_{12,12} = 0.$$